

Tuning the probability of defect formation via substrate strains in Sr₂FeMoO₆ films

Waheed A. Adeagbo,^{1,*} Martin Hoffmann,^{2,†} Arthur Ernst,^{2,3} Wolfram Hergert,¹ Minnamari Saloaro,⁴ Petriina Paturi,⁴ and Kalevi Kokko^{5,6}

¹*Institute of Physics, Martin Luther University Halle-Wittenberg, Von-Seckendorff-Platz 1, 06120 Halle, Germany*

²*Institute for Theoretical Physics, Johannes Kepler University Linz, Altenberger Straße 69, 4040 Linz, Austria*

³*Max Planck Institute of Microstructure Physics, Weinberg 2, 06120 Halle, Germany*

⁴*Wihuri Physical Laboratory, Department of Physics and Astronomy, University of Turku, FI-20014 Turku, Finland*

⁵*Department of Physics and Astronomy, University of Turku, FIN-20014 Turku, Finland*

⁶*Turku University Centre for Materials and Surfaces (MatSurf), Turku, Finland*



(Received 14 May 2018; revised manuscript received 3 July 2018; published 10 August 2018)

Since oxide materials like Sr₂FeMoO₆ are usually applied as thin films, we studied the effect of biaxial strain, resulting from the substrate, on the electronic and magnetic properties and, in particular, on the formation energy of point defects. From our first-principles calculations, we determined that the probability of forming point defects, like vacancies or substitutions, in Sr₂FeMoO₆ could be adjusted by choosing a proper substrate. For example, the amount of antisite disorder can be reduced with compressive strain in order to obtain purer Sr₂FeMoO₆ as needed for spintronic applications, while the formation of oxygen vacancies is more likely for tensile strain, which improves the functionality of Sr₂FeMoO₆ as a basis material of solid oxide fuel cells. In addition, we were also able to include the oxygen partial pressure in our study by using its thermodynamic connection with the chemical potential. Strontium vacancies become, for example, more likely than oxygen vacancies at a pressure of 1 bar. Hence, this degree of freedom might offer in general another potential method for defect engineering in oxides aside from, e.g., experimental growth conditions like temperature or gas pressure.

DOI: [10.1103/PhysRevMaterials.2.083604](https://doi.org/10.1103/PhysRevMaterials.2.083604)

I. INTRODUCTION

Lattice imperfections like point defects can be crucial for the functionality of novel materials. They can destroy desired properties but might also improve or even just allow new functionalities. A good example is the double-perovskite material Sr₂Fe_{1+x}Mo_{1-x}O_{6-δ}, where x symbolizes nonstoichiometry at the B/B' site and δ oxygen deficiency (general formula $A_2B'B'O_6$). It is a versatile material, which is throughout literature considered for several potential applications.

For example, the half-metallic character of Sr₂FeMoO₆ (SFMO), which is experimentally observed as promising high-spin polarization [1], is a highly desired property in order to access spintronics [2,3]. Besides, SFMO shows a low-field magnetoresistance response, a magnetic transition above ambient temperatures [4], and a high magnetic moment per functional unit in a range of $2.2\mu_B/\text{f.u.}$ to $3.9\mu_B/\text{f.u.}$ [5–8]. Nevertheless, a successful utilization of SFMO is still problematic since the theoretical predicted half-metallicity [9], which is one requirement of its high-spin polarization, is usually diminished or even lost in thin-film samples of Sr₂FeMoO₆ [10–13]. This deterioration effect was attributed to doping, defects, grain boundaries, or parasitic phases, so that, e.g., the saturation magnetization becomes strongly reduced compared with its theoretically expected value. The latter should be $4\mu_B/\text{f.u.}$ arising from the spin quantum number of $S = \frac{5}{2}$ of

the Fe³⁺ ions and the antiparallel coupled electrons with $S = \frac{1}{2}$ from the Mo⁵⁺ ions [9]. It was verified in many theoretical studies, which shed light upon the microscopic origins of the magnetic properties of SFMO and their alterations [14–20]. While oxygen vacancies, a common observation in transition-metal oxides, seem not to interfere with the spin polarization of SFMO [13,20–22], the stoichiometry-preserving exchange of B and B' atoms, so-called antisite disorder (ASD), can strongly reduce the saturation magnetization, the spin polarization [21–23], the magnetotransport properties [24,25], or might even influence long-range magnetic ordering [26,27]. Hence, a synthesis of Sr₂FeMoO₆ samples is rather difficult because of a non-negligible concentration of defects. Therefore, there is a strong desire to control the amount of defects in Sr₂FeMoO₆ samples [11,13].

On the other hand, the easy formation of oxygen vacancies in Sr₂FeMoO₆ makes it a good candidate as mixed ionic electronic conductor in solid oxide fuel cells (SOFC) [20,28]. Experimental studies investigate its potential as anodes with a nonstoichiometric ratio between Fe and Mo [29,30], while theoretical studies calculate the oxygen diffusion [31] or the formation energy of oxygen vacancies in bulk Sr₂FeMoO₆ [20].

Both applications utilize thin films of SFMO [13,32], where the substrate might cause epitaxial biaxial strain, another factor deteriorating the desired properties of the SFMO film [33]. Although very large biaxial strains could theoretically induce a spin transition in bulk SFMO [34], our recent study revealed not only that a compressive biaxial strain $\sim 1\%$ at SrTiO₃ substrates does not show any significant direct impact on the magnetic

*waheed.adeagbo@physik.uni-halle.de

†martin.hoffmann@jku.at

properties of SFMO [13], but also that the amount of ASD and oxygen vacancies is reduced compared to the observed defect concentrations in the SFMO bulk target from which the films were grown [13].

This increase of defect formation probabilities was an interesting experimental finding. Hence, we want to study the role of biaxial strain in SFMO further in more detail. In particular, oxygen vacancies are one way for various oxides to compensate tensile strain since the observed chemical expansion can accommodate parts of the strain [35,36]. It could mean therefore potentially room-temperature magnetism for SFMO thin films due to tensile biaxial strain because oxygen vacancies were shown to increase the Curie temperature in SFMO as well [37].

However, other point defects than oxygen vacancies were only rarely discussed in literature on strained oxide materials. We carried out density functional theory (DFT) calculations in order to study systematically the structural and magnetic properties of SFMO including various point defects under the influence of biaxial strain, in particular, ASD and other vacancies. We observe strong variations of formation energies up to 1 eV depending on the kind of considered defect allowing for potential defect engineering with the decision for a particular substrate.

II. TECHNICAL DETAILS

Our calculations are performed using the Vienna *ab initio* simulation package (VASP) [38,39]. While we present here only setup information, which are deviating from a standard VASP setup used, e.g., in previous theoretical studies on SFMO [20,22], we provide further numerical details and parameters in the Supplemental Material [40].

We used in our calculations the tetragonal unit cell containing two functional units (f.u.) of $\text{Sr}_2\text{FeMoO}_6$ [Figs. 1(a) and 1(b)] and a supercell comprising 8 f.u. of $\text{Sr}_2\text{FeMoO}_6$, in total 80 atoms [Figs. 1(c) and 1(d)]. Both structures stabilize after numerical relaxation in the space group $I4/m$, which is in agreement with experimental observations and shows oxygen octahedra, which rotate only slightly in the xy plane and remain static otherwise (Fig. 1). The Fe octahedra are rotated clockwise by $\beta = 7.43^\circ$ while the Mo octahedra rotate counterclockwise.

Former theoretical studies [19,20,22,34] discuss correlation corrections GGA + U as the crucial factor in order to obtain for SFMO a total magnetic moment of $4.0\mu_B/\text{f.u.}$, but we will show below that this is also achieved with the fixed spin moment method (FSM) [42,43] and a generalized gradient approximation (GGA) functional alone. FSM allows a constrained calculation fixing the total spin magnetic moment for the considered cell (see [40] for an example of VASP input parameters). Hence, the total energy of the system depends not only from the volume alone, but is now an explicit function of the total magnetic moment as well. This offers a method for studying materials where the magnetic moments can change discontinuously with volume and ranges of coexistence for different magnetic phases might exist, maybe exhibiting metamagnetic behavior [44]. In order to obtain the ground state and spin configuration of the system in dependence of this two-dimensional total-energy landscape $E(m_{\text{tot}}, V)$, we

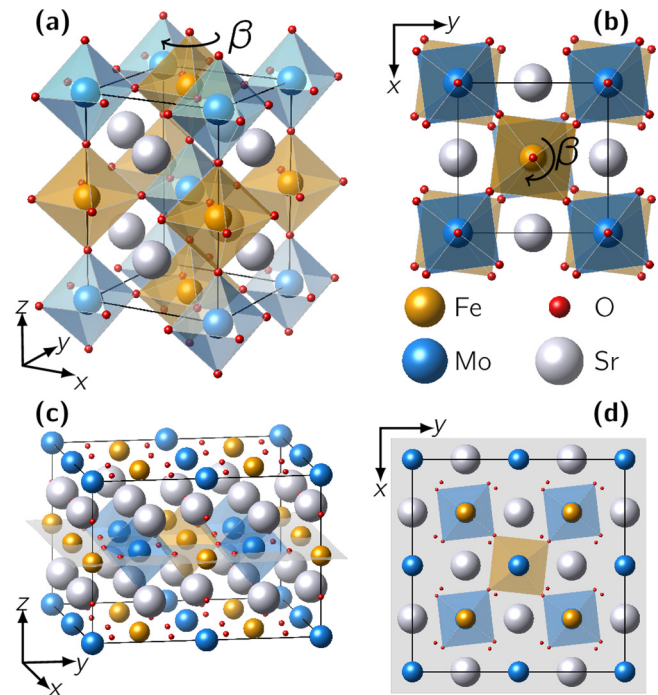


FIG. 1. Considered lattice structures of $\text{Sr}_2\text{FeMoO}_6$. (a) Tetragonal unit cell with $I4/m$ symmetry visualizing the octahedral environment of Fe and Mo formed by the oxygen atoms with colored polyhedra. (b) Top view showing the octahedra rotation denoted as β and counted in clockwise direction for the Fe ion octahedron. (c) Side view of the $2 \times 2 \times 1$ supercell with 8 f.u. used for the defect calculations. (d) Top view of the supercell in (c) from the gray xy layer downwards. Structural figures were prepared with VESTA [41].

imposed with FSM a total magnetic moment m_{tot} varying from $3.5\mu_B$ to $4.3\mu_B$ on the defect-free tetragonal SFMO unit cell, let the structural and internal parameters relax, and calculated the total energy (see [40] for the total energy of a single Mo vacancy at different total magnetic moments). We released then as a test the magnetic constrain after finding the ground-state structure, but no further relaxation was observed and the ground state remained the same. FSM was in particular important for calculations at large compressive or tensile strain where the total-energy landscape can be strongly varied and several different competing magnetic phases might appear.

III. GROUND-STATE PROPERTIES WITH FIXED SPIN MOMENT METHOD

At first, we studied defect-free SFMO in order to demonstrate that FSM is able to reproduce the correct ground-state properties of SFMO. The configuration with a net magnetic moment of $m_{\text{gs}} = 4.0\mu_B/\text{f.u.}$ had finally the lowest total energy and is, therefore, the ground state at 0 K for defect-free unstrained SFMO. We have to note that this ground state shows directly the half-metallic density of states (DOS) with only spin-down states at the Fermi energy (Fig. 2). The spin-up band gap for defect-free, unstrained SFMO is 1.3 eV measured between the unoccupied Mo t_{2g}^{\uparrow} and the occupied Fe e_g^{\uparrow} . It is smaller than reported elsewhere [20] but agrees well with the available experimental values (0.5 eV, 1.3 eV) in [7,45].

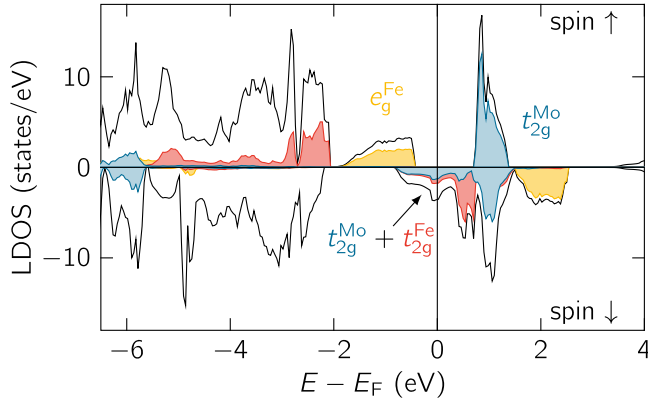


FIG. 2. Spin-resolved local density of states (LDOS) of unstrained and defect-free SFMO calculated with FSM in VASP.

The first one represents an optical measurement, while the second experimental band gap follows from photoemission spectroscopy. Of course, we have to consider also a thermal broadening of the electronic states with increasing temperature when comparing the size of the theoretical and experimental band gap. In the spin-down channel, the Mo t_{2g}^{\downarrow} and Fe t_{2g}^{\downarrow} states hybridize around the Fermi energy (Fig. 2).

That means that the internal structure relaxes under the magnetic constrain to positions, which exhibit the correct electronic and magnetic properties, give the lowest total energy, and remain stable also after releasing the constraint. We have indeed seen already that the properties of SFMO are rather sensitive to small local relaxations in particular by the specific distances in the Fe-O-Mo bonds [46]. We assume that the magnetic constraint opens a relaxation path to a lattice structure, which is usually not easily available from another starting point. In a same way, the GGA + U could have allowed the correct relaxation, not possible from a normal spin-polarized start setup [20]. After stabilizing the lattice structure, one reaches in both cases a minimum in the energy landscape with similar material properties.

The application of correlation corrections within GGA + U ($U = 4$ eV on Fe $3d$ orbitals) on top of FSM leads then only to a wider half-metallic band gap (from 1.3 to 2.4 eV). Only the Fe e_g^{\uparrow} states are shifted to lower energies. The magnetic moment at the Fe site increases from $m_{Fe} = 3.6\mu_B/\text{f.u.}$ to $3.8\mu_B/\text{f.u.}$, but the ground state does not change. The application of correlation corrections to the Mo d states was neglected because we observed in test calculations only small shifts of the states in the conduction band, which had no effect on the magnetic moments or structural relaxations. Therefore, we followed earlier studies [20,47].

Indeed, also the corresponding lattice parameters of defect-free SFMO at the ground state ($a = b = 5.55$ Å and $c = 7.90$ Å) agree very well with various experimental results [11,48–50] for FSM alone (Table I). In fact, they are the same as the lattice parameters measured at 70 K [51] ($a = 5.5521$ Å and $c = 7.9013$ Å). This agreement is much better than what can be achieved by the GGA + U method obtained earlier [19,20,34] (see also our results in Table I).

We calculated also the bulk modulus B_0 via the hydrostatic pressure but available experimental data [48,49] are much

TABLE I. Structural properties of defect-free, unstrained $\text{Sr}_2\text{FeMoO}_6$ with FSM: bulk modulus B_0 , Grüneisen constant B'_0 , and the lattice parameters. The units are given in parentheses, while B'_0 is dimensionless. Experimental results for polycrystalline $\text{Sr}_2\text{FeMoO}_6$ samples obtained at room temperature vary in grain size from 50 or 100 nm [48] to ~ 2 μm [49].

	GGA	GGA + U	Experiment [48,49]		
B_0 (GPa)	147.42	152.80	266 ± 3	284 ± 6	331 ± 12
B'_0	4.68	4.44	4.0	4.0	4.0
a (Å)	5.5522	5.6378	5.5703	5.5791	5.5703
c (Å)	7.9013	7.9731	7.7879	7.8698	7.8832
Grain size (nm)			~ 2000	100	50

larger than the numerical value (Table I). However, we note that these experimental bulk moduli were determined with polycrystalline samples and the bulk modulus decreases strongly by 65 GPa with increasing the grain size from 50 nm to 2 μm. We can interpret our theoretical *ab initio* calculation as a kind of limit to the infinite large grain size, which could then validate the bulk modulus (147 to 153 GPa) obtained in our and former calculations [20]. Applying additional correlation corrections (GGA + U) shows here only small variations ~ 5 GPa (Table I).

Finally, we determined the elastic tensor of the tetragonal structure by six independent single-crystal elastic constants: c_{11} , c_{12} , c_{13} , c_{33} , c_{44} , and c_{66} (Table II). Experimentally determined elastic constants were unfortunately not available, but theoretical values for other double perovskites do not deviate far from our results (Table II): Ba_2MgWO_6 has $c_{11} = 256.2$ GPa, $c_{12} = 85.8$ GPa, $c_{44} = 95.3$ GPa, and $B_0 = 143.1$ GPa [52]; or $\text{Sr}_2\text{CaOsO}_6$ has $c_{11} = 331.19$ GPa, $c_{12} = 77.47$ GPa, $c_{44} = 63.35$ GPa, and $B_0 = 162.04$ GPa [53]. For GGA + U , the c_{ij} of SFMO, except of c_{66} , vary by less than $\leq 10\%$ (Table II).

We conclude that the GGA and FSM are indeed a valid tool to calculate the ground-state properties for this particular magnetic material, while the additional usage of correlation corrections does not influence the ground-state properties strongly or even describes them wrongly. Even the difference between the total energies needed for the defect formation energies are small for a range of moderate biaxial strains used below [40]. Hence, we applied FSM in all further calculations including biaxial strain and/or defects: (a) We set a total magnetic moment for the unit cell and calculated the structural relaxation. (b) For a set of varying magnetic moments, we defined the structure with the lowest total energy as the most stable structural and magnetic configuration with total magnetic moment m_{gs} [40]. If needed for reasons of

TABLE II. Single-crystal elastic constants c_{ij} of defect-free, unstrained $\text{Sr}_2\text{FeMoO}_6$ with FSM written in Voigt notation and in GPa.

	c_{11}	c_{12}	c_{13}	c_{33}	c_{44}	c_{66}
GGA	230.32	77.70	108.93	244.42	45.48	63.95
GGA + U	245.54	82.97	109.00	267.97	48.489	76.61

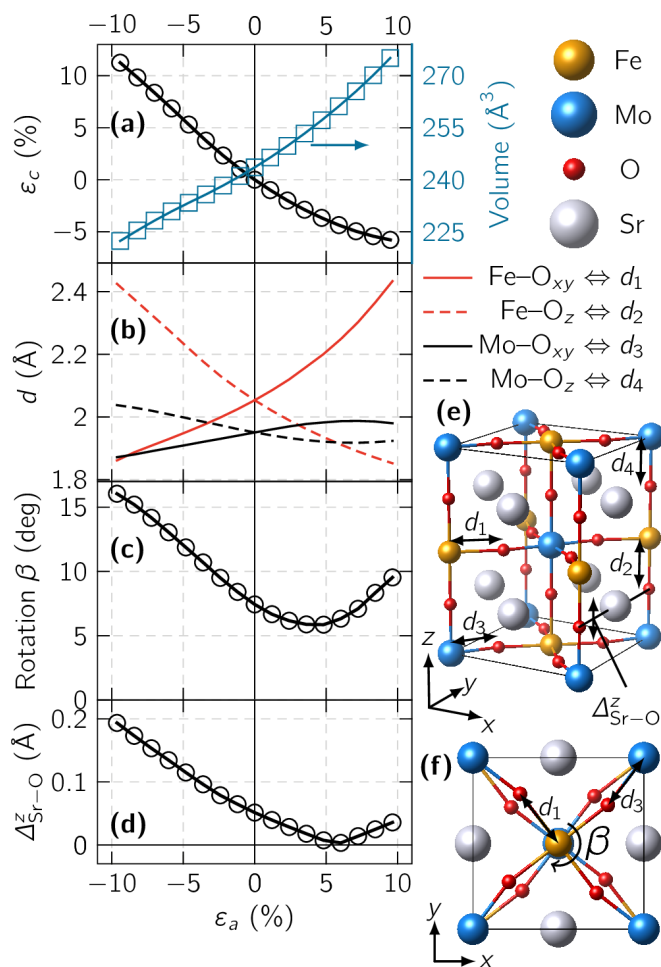


FIG. 3. Structural variation with biaxial strain in the lattice constants $a = b$. (a) Variation of lattice parameter c and the volume of the tetragonal cell. (b) The in-plane (xy) and out-of-plane z bond lengths Mo-O and Fe-O. (c) Octahedra rotation angle β , visualized in (f). (d) Out-of-plane distances between Sr and O. (e), (f) Visualization of distances and angles in the tetragonal unit cell. Structural figures were prepared with VESTA [41].

comparison, we will mention explicitly the use of correlation corrections (GGA + U).

IV. VARIATIONS IN BULK SFMO WITH BIAxIAL STRAIN

In our previous study [13], only calculations at selected biaxial strain values were considered. Here in this work, we continued with a comprehensive study of SFMO for a larger range of biaxial strain going from -10% to 10% . The structural and magnetic configuration at zero strain is represented by the tetragonal ground-state structure [Fig. 1(a)] as described above and the biaxial strain was applied by fixing the in-plane lattice constants ($a = b$) and relaxing the out-of-plane lattice constants (c) and the internal parameters (Fig. 3). Although a similar study was already published by Lu *et al.* [34], we present the variations of the structural and magnetic properties of SFMO with biaxial strain as the basis for the later discussion of the formation energy of point defects. In addition, we used a different numerical treatment, namely FSM, while Lu *et al.* [34] used the GGA + U method with $U = 4$ eV.

At each applied biaxial strain, we ensured the true ground-state properties using FSM as described above. We characterized the corresponding structural variation by analyzing the volume, Fe-O and Mo-O bond lengths, the different height of Sr and O ions, and the octahedra rotation angles with biaxial strain. As observed already for other oxides [35,36], SFMO does not follow the Poisson ratio but rather its volume becomes reduced (increased) for compressive (tensile) biaxial strain [Fig. 3(a)]. The in-plane (xy) and out-of-plane (z) Fe-O bond lengths [red marks in Fig. 3(b), distances d_1 and d_2 in Figs. 3(e) and 3(f)] vary considerably more than the Mo-O bond lengths [black marks in Fig. 3(b), distances d_3 and d_4 in Figs. 3(e) and 3(f)], while their values of 2.053 and 1.951 Å, respectively, for unstrained SFMO agree well with experimental values [50]. The bond lengths follow the natural tendency, the in-plane contributions become smaller with compressive biaxial strain and elongated for tensile biaxial strain, while it is vice versa for the out-of-plane bond lengths. The oxygen ions hybridize stronger with the 4d states of Mo than with the 3d states of Fe. Already Solovyev [46] found that a smaller Mo-O bond length should be the natural state of SFMO. The bond lengths are also connected with the rotation angles of the oxygen octahedra [angle β in Fig. 3(f)]. The rotation becomes larger under compressive biaxial strain [Fig. 3(c)]. Hence, the additional octahedra rotation is another mechanism in order to compensate the in-plane biaxial strain [35]. In z direction, the elongation caused by the compressive in-plane strain causes the oxygen ions to hybridize even stronger with Mo, while the Fe-O bond becomes much larger [Fig. 3(b)]. The octahedra experience even stronger breathing distortions than in the ground state [46]. The other oxygen ions in the xy plane of Sr-O avoid in a similar way the compressive strain by relaxing out of that plane [Fig. 3(d)]. Interestingly, the oxygen ions do not relax closer to the Fe ions but form an ideal plane with Sr and relax out of the plane again for larger tensile strains.

These internal structural changes influence of course magnetic and electronic properties as it was observed already earlier [34]. Using FSM, we obtain only small variations for the magnetic properties for the experimental relevant range of $\pm 4\%$ biaxial strains (Fig. 4). The Fe ions keep their high-spin state with a maximal local magnetic moment of $3.63\mu_B/f.u.$ at zero strain (unstrained SFMO), which is only slightly diminished for both strains, compressive or tensile, in agreement with the conclusions of Lu *et al.* [34] [Fig. 4(a)]. The same holds true for the antiparallely aligned magnetic moments at the Mo ions: the absolute value is slightly reduced [Fig. 4(b)]. The local magnetic moments at the oxygen ions follow the opposite tendency of their bond lengths with the Fe and Mo ions [Fig. 3(b)]. The local moment increases, if the bond length is reduced, and decreases, if the bond length is elongated [Fig. 4(c)].

The situation changes for compressive strains, which are larger than -4% . Here, we obtained a transition to a completely metallic state because the band gap in the majority-spin channel $\Delta_{\uparrow}E$ closes [marked with a vertical dashed line in Fig. 4(d)]. With the compressive biaxial strain, the Fe e_g^{\uparrow} states are almost linearly shifted towards the Fermi energy E_F [see inset in Fig. 4(h) and [40]]. At that strain value when the Fe e_g^{\uparrow} state “hits” the Fermi energy, a kind of “jump” seems to appear. This only follows from the fact that $\Delta_{\uparrow}E$ is measured from the Fe

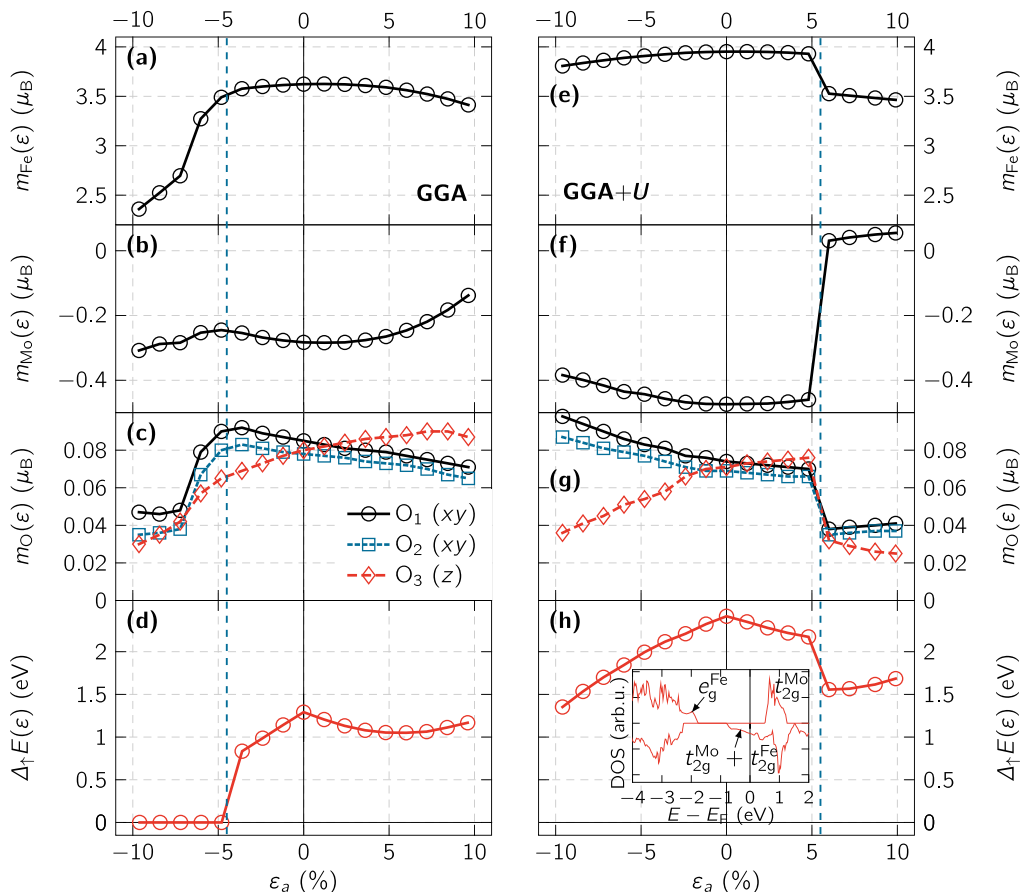


FIG. 4. Variations of magnetic and electronic properties with biaxial strain for GGA and GGA + U . The local magnetic moments for (a), (e) Fe ions, (b), (f) Mo ions, and (c), (g) O ions. (d), (h) Band gap in the majority-spin channel calculated from the density of states (DOS). The inset shows the DOS for unstrained defect-free SFMO. The vertical dashed line at -4.5% on the left-hand side marks the spin transition from half-metallic high-spin state to metallic low-spin state. The vertical dashed line at 5.5% on the right-hand side marks the transition from ferrimagnetic (FIM) to ferromagnetic (FM) state.

e_g^\uparrow states to the Mo t_{2g}^\uparrow states. The position of the unoccupied Mo t_{2g}^\uparrow states does not change.

This result contradicts Lu *et al.* [34], who observed instead a half-metallic state with a spin transition from high spin to intermediate spin of the local moment at the Fe ion. Hence, we present also calculations with FSM including correlations corrections via GGA + U (right side of Fig. 4). The combination of FSM and GGA + U allows to determine accurately the magnetic ground state of SFMO. For compressive biaxial strain, we neither observe a spin transition nor a half-metal to metal transition [Fig. 4(h)]. The Fe e_g^\uparrow states are now much further below the Fermi energy and 10% compressive strain is not enough to shift them far enough. We can only guess that the spin transition could be another local minimum in the energy landscape of SFMO, while FSM ensures the correct magnetic ground state.

On the other hand, the spin transition in the tensile strain region at $\sim 5\%$ [marked with a vertical dashed line in Fig. 4(h)], which is as well reported by Lu *et al.* [34] for $\sim 7\%$ seems to be a stable magnetic phase transition when applying U but does not appear otherwise. While the exact biaxial strain value of the transition may vary with FSM treatment, the ferrimagnetic state becomes ferromagnetic (FIM-FM transition).

The magnetic moment of Fe ions decreases from $3.95\mu_B/\text{f.u.}$ to $3.50\mu_B/\text{f.u.}$, while the Mo ions go into a low-spin state [34] and their local moments align parallel with the magnetic moments of the Fe ions [Fig. 4(e)].

Hence, we can conclude that the observed variations in the electronic and magnetic properties are rather small and not yet relevant in experimental conditions for SFMO (moderate strain values of -4% to 4%) [13]. Nevertheless, we can observe an important effect of biaxial strain for the formation of point defects demonstrated in the next section.

V. POINT DEFECTS IN SFMO WITH BIAXIAL STRAIN

Using the supercell consisting of $2 \times 2 \times 1$ tetragonal unit cells and 80 atoms [Fig. 1(c)], we calculated the defect formation energies of different point defects D following Nayak *et al.* [54] and considered in addition a strain ε dependence as $E_{\text{form}}(D, \varepsilon)$. We briefly recall the technical details of determining the defect formation energy from the DFT total energies in the Supplemental Material [40].

We considered aside from common defect configurations such as oxygen vacancies (V_O) and antisite disorder (ASD) also cation vacancies of Mo (V_{Mo}), Fe (V_{Fe}), Sr (V_{Sr}), as well as nonstoichiometric disorder, a Fe ion at a Mo sublattice

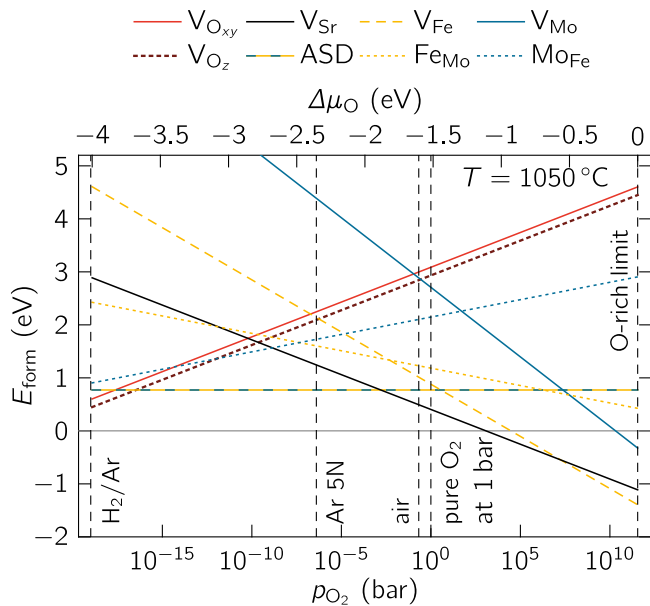


FIG. 5. Defect formation energy of defects in unstrained SFMO ($\varepsilon = 0$) for varying oxygen partial pressure at $T = 1050^\circ\text{C}$. The relative chemical potential is shown at the upper axis. The legend is given above the figure.

(Fe_{Mo}) or a Mo ion at a Fe sublattice (Mo_{Fe}). We took also into account the two nonequivalent oxygen positions, in-plane (O_{xy}) and out-of-plane (O_{z}) (Fig. 3), since the properties of the corresponding vacancies $\text{V}_{\text{O}_{\text{xy}}}$ and $\text{V}_{\text{O}_{\text{z}}}$, respectively, might change considerably, as shown for CaMnO_3 [35]. We note that the absolute values of formation energies are limited to the choice of the chemical potentials μ_i of defect species i , since the chemical potentials exactly suitable to the experimental growth conditions are unknown.

We took as reference point the chemical potentials of the respective oxides for all the chemical elements in SFMO (SrO , Fe_2O_3 , MoO_2) and the oxygen-rich condition $\mu_{\text{O}}^{\text{max}}$ for the oxygen chemical potential [40]. In addition, the oxygen chemical potential can be varied as a parameter in order to simulate experiments at different oxygen partial pressure using thermodynamic considerations [40,54,55]. The results are straight lines with the slope $\propto \Delta\mu_{\text{O}} = \mu_{\text{O}} - \mu_{\text{O}}^{\text{max}}$ and $E_{\text{form}}(D, \varepsilon = 0)$ at $\Delta\mu_{\text{O}} = 0$ (Fig. 5). At a first glance, SFMO appears even not stable within our choice of reference chemical potentials: removing a single metal ion for a vacancy is favored and the defect formation energy $E_{\text{form}}(D, \varepsilon, \Delta\mu_{\text{O}} = 0)$ is negative for V_{Fe} , V_{Sr} , and V_{Mo} . Here, it is not surprising that both types of oxygen vacancies $\text{V}_{\text{O}_{\text{xy}}}$, $\text{V}_{\text{O}_{\text{z}}}$ (reddish lines) are in the oxygen-rich regime less probable. With less oxygen partial pressure, the formation energy of all metal vacancies increases and their appearance gets more unlikely while SFMO becomes more stable. Just at very low partial pressures ($\sim \text{H}_2/\text{Ar}$ atmosphere), the formation energy of oxygen vacancies becomes comparable with the one of ASD. We can conclude that the relative probability of point defects is very sensitive to the exact experimental conditions.

We are well aware of other choices for reference chemical potentials of multicomponent compounds using, e.g., the concept of constitutional defects developed by Hagen

and Finnis for ordered alloys [56], which was applied for $\text{Sr}_2\text{FeMoO}_6$ [19]. There, the extreme case of Mo-rich (Mo_{Fe}) or Fe-rich Fe_{Mo} was used as references [19], which makes a direct comparison complicated and we restrict ourselves to the comparison of the electronic structure as discussed above.

At first, we verified for strain-free SFMO that GGA and FSM are applicable and we can avoid computational heavy calculations with, e.g., hybrid-functional methods, which might raise ambiguities for the calculations of defect formation energies or need postprocessing as discussed in [54]. In particular, the choice of a specific U for GGA + U calculations cannot be simply transferred to any of the reference systems used to determine the formation energy. A recent work comparing for an oxide heterostructure a diffusion quantum Monte Carlo method with DFT calculations [57] shows that the absolute value of the formation energies of oxygen vacancies can vary by few electron volts. Nevertheless, the overall and relative tendency between different defects is conserved throughout various U values or functionals. Hence, we crosschecked again the electronic structure including now the different defects in the supercell. We observe that in agreement with other theoretical studies [19,20,22] only in the case of oxygen, iron, or strontium vacancies, no additional states form in the spin-up channel at the Fermi energy and the DOS remains half-metallic [40].

The formation energies at biaxial strains follow then by considering total energies of the relaxed supercells including defects, scaled with respect to the defect-free, ground-state total energy for a series of biaxial strains (-6% to $+6\%$). We note that for compressive strains $< -4\%$, the observed spin transition, discussed in the last section (Fig. 4), might cause also changes in the formation energy, which would be hard to separate from purely strain-mediated effects. Different oxygen partial pressure just scales all lines by an additive term depending on the respective chemical potentials with $\Delta\mu_{\text{O}}$ or p_{O_2} (Fig. 5). Hence, we obtained that the applied biaxial strain lowers for both oxygen vacancy types, $\text{V}_{\text{O}_{\text{xy}}}$ and $\text{V}_{\text{O}_{\text{z}}}$, the formation energy and increases the probability of oxygen vacancies, with a more pronounced effect in the tensile strain region and for the out-of-plane oxygen vacancy $\text{V}_{\text{O}_{\text{z}}}$ [Fig. 6(a)]. Although the order of $\text{V}_{\text{O}_{\text{xy}}}$ and $\text{V}_{\text{O}_{\text{z}}}$ is swapped, we can see a similarity with the formation energies in, e.g., CaMnO_3 [35]. The formation of oxygen vacancies is easier in the tensile strain region because the ionic radii of Fe and Mo ions increase with lower valency [58] causing a larger overall volume similar to the Mn ions in CaMnO_3 . A direct comparison will be, however, complicated. We can also expect different intrinsic strain relaxation mechanism in the largely distorted perovskite structure of CaMnO_3 compared with the less distorted SFMO structure. Nevertheless, we can state that the oxygen vacancy formation is easier in biaxial strained films. This will be an advantage not only for solid oxide fuel cells but also for the magnetic properties of SFMO, since we found recently that the Curie temperature can be strongly enhanced by oxygen vacancies in SFMO [37].

On the contrary, the formation energies of antisite defects increase for a large range of biaxial strain, e.g. [increase of $E_{\text{form}}(D)$], by $+386$ and $+78$ meV for compressive or tensile strains $\varepsilon = \pm 3\%$ (Fig. 6). It only becomes reduced by -48 meV for small tensile strains in the range of $0 < \varepsilon < 3\%$

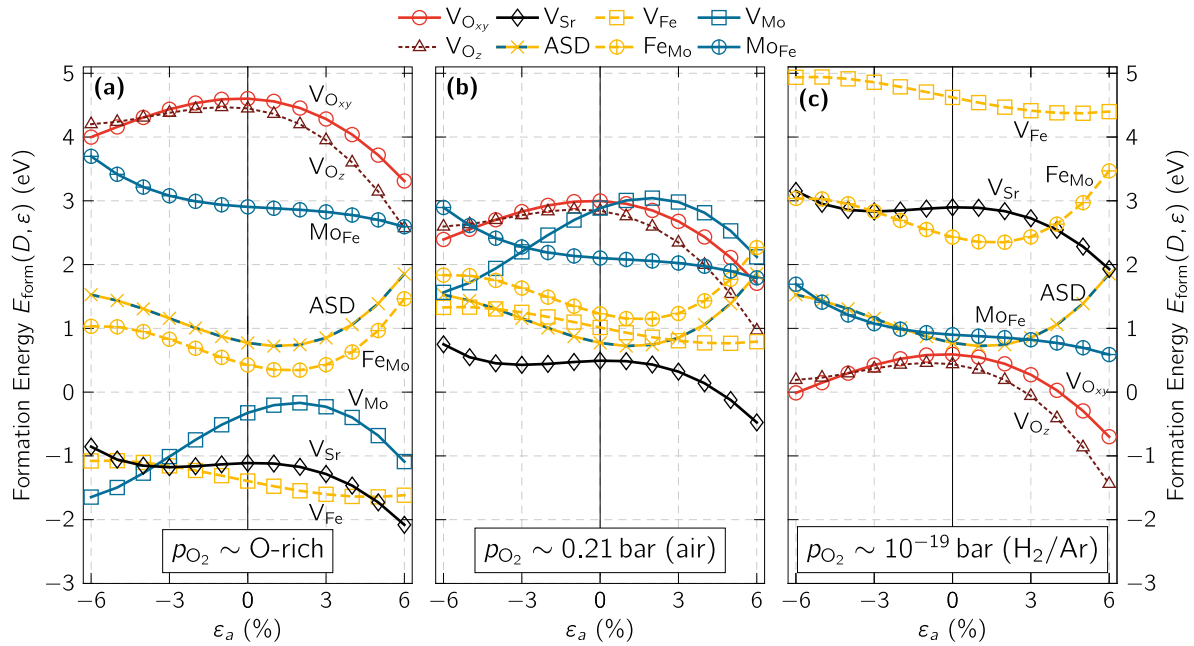


FIG. 6. Formation energies of defects in dependence of biaxial strain and three different oxygen partial pressures. The legend is given above the figure. V_{Mo} is out of range in (c).

and gets again larger for tensile strains $>2\%$. That means that, in terms of applications, biaxial strained films should be more ordered and better samples for spintronic applications [13]. This can be related to already made experimental observations on ASD. Various experiments investigated the A site substitution in double perovskites ($A_2BB'O_6$) and its influence to magnetization, spin polarization, ASD, etc. Chan *et al.* [16] found a chemical pressure in SFMO, when substituting Sr with Ca (ionic radii are 1.34 Å for Ca^{2+} and 1.44 Å for Sr^{2+} [58]), which caused an increase in magnetic moment but also a pronounced decrease in ASD. Hence, compression can, aside from the chemical variations from Sr to Ca, reduce the number of antisite defects. Kahoul *et al.* [18] observed on the other hand an increase in the lattice constant of SFMO, when doping Sr with La. This raised also the measured amount of ASD but was only indirectly related with the doping via electronic effects since the ionic radius of La^{3+} (1.36 Å) is smaller than that of Sr^{2+} [18,59]. Although the effects of chemical substitution could overlay effects caused by a lattice constant variation, these experiments include hints of our theoretical observations.

Considering the other defects, we found that V_{Sr} , V_{Fe} , and Mo_{Fe} are less influenced by the biaxial strains -3% to 3% . Only $E_{form}(V_{Sr}, \epsilon)$ lowers considerably (-1 eV) for larger tensile strains, which then favors V_{Sr} over V_{Fe} [Fig. 6(a)]. Moreover, ASD can be considered as a defect complex of the two nonstoichiometric defects Mo_{Fe} and Fe_{Mo} . The average of their formation energies taking into account the oxygen chemical potential properly matches the one of the antisite defects. The high formation energy of Mo_{Fe} is, however, surprising because we would expect substitution of Fe with Mo much more likely since $SrMoO_x$ is a typical impurity phase when growing SFMO films [60,61].

This discrepancy is resolved when we consider lower oxygen partial pressures, e.g., at ambient air pressure [Fig. 6(b)]

or almost vacuum [Fig. 6(c)]. Not only do V_{Oxy} become more and V_{Mo} less likely, also all formation energies shift to positive formation energies at $\epsilon = 0$. The latter means that there are no spontaneous vacancies anymore and SFMO is indeed stable. Only at large tensile strains, $E_{form}(V_{Sr})$ still gets below zero. This means that biaxial strains could significantly alter the energy landscape, the relative order of the defect formation energies or their crossing points (better visible in Fig. 5). The low $E_{form}(V_{Sr})$ also means that V_{Sr} are likely to appear in SFMO for a large range of experimental conditions. Therefore, Sr vacancies could be more important than earlier expected and might also deteriorate the magnetic properties of SFMO [62]. Also, the formation of Mo oxide impurity phases is more likely at ambient air partial pressure: Fe vacancies could form easier and can be filled by Mo (Mo_{Fe}).

When going to lower partial pressures, antisite defects become the most likely defect [Figs. 5 and 6(b)] and only for partial pressures smaller than 10^{-16} bar oxygen vacancies will be the most probable defect type [Fig. 6(c)]. Then, nonstoichiometric Mo at an Fe site has an almost similar probability to form than an antisite defect. This means that $SrMoO_x$ impurity phases become more likely close to vacuum.

VI. CONCLUSIONS

Although the absolute values of the defect formation energies might alter with another choice of reference point for the chemical potential of the single elements, we could observe a pronounced effect of realistic biaxial strains on the point-defect profile of oxide materials, here Sr_2FeMoO_6 , via a strong influence on the defect stability [$E_{form}(D, \epsilon)$ varies by ~ 0.2 eV per 1% strain]. The half-metallic ground state of defect-free SFMO will be preserved at moderate strains, but the relative order of formation energies for different defects might be altered, e.g., V_{Fe} vs V_{Sr} or V_{Oxy} vs V_{Oz} .

Most interestingly, the amount of antisite defect formation can be reduced in compressively strained SFMO films and oxygen vacancies will form easier under both strains, compressive and tensile. Latter defects are crucial for solid oxide fuel cells or can enhance magnetic properties in SFMO [13,37].

Taking into account also the oxygen partial pressure as an experimental parameter offers another degree of freedom for the defect formation energies. Our numerical results at partial pressures matching air or vacuum atmosphere can be compared directly with experimental measurements. We found that V_{Sr} are very likely over a large range of partial pressures, while oxygen vacancies become most likely only for very

low partial pressures $<10^{-16}$ bar. Hence, we have demonstrated the potential of targeted first-principles calculations in designing strain-defect engineering processes for the tuning of the properties of SFMO or other oxides.

ACKNOWLEDGMENTS

This publication was funded by the German Research Foundation within the Collaborative Research Centre 762 (Projects No. A4 and No. B1). The Jenny and Antti Wihuri Foundation is acknowledged for financial support.

-
- [1] R. P. Panguluri, S. Xu, Y. Moritomo, I. V. Solovyev, and B. Nadgorny, *Appl. Phys. Lett.* **94**, 012501 (2009).
- [2] M. Bibes, K. Bouzehouane, A. Barthélémy, M. Besse, S. Fusil, M. Bowen, P. Seneor, J. Carrey, V. Cros, A. Vaurès, J.-P. Contour, and A. Fert, *Appl. Phys. Lett.* **83**, 2629 (2003).
- [3] A. Nag, S. Jana, S. Middey, and S. Ray, *Indian J. Phys.* **91**, 883 (2017).
- [4] J. Fontcuberta, D. Rubi, C. Frontera, J. L. García-Muñoz, M. Wojcik, E. Jedryka, S. Nadolski, M. Izquierdo, J. Avila, and M. C. Asensio, *J. Magn. Magn. Mater.* **290-291 PA**, 974 (2005).
- [5] H. Q. Yin, J. S. Zhou, J. P. Zhou, R. Dass, J. T. McDevitt, and J. B. Goodenough, *Appl. Phys. Lett.* **75**, 2812 (1999).
- [6] T. Manako, M. Izumi, Y. Konishi, K.-I. Kobayashi, M. Kawasaki, and Y. Tokura, *Appl. Phys. Lett.* **74**, 2215 (1999).
- [7] Y. Tomioka, T. Okuda, Y. Okimoto, R. Kumai, K.-I. Kobayashi, and Y. Tokura, *Phys. Rev. B* **61**, 422 (2000).
- [8] A. Di Trolio, R. Larciprete, A. M. Testa, D. Fiorani, P. Imperatori, S. Turchini, and N. Zema, *J. Appl. Phys.* **100**, 013907 (2006).
- [9] K.-I. Kobayashi, T. Kimura, H. Sawada, K. Terakura, and Y. Tokura, *Nature (London)* **395**, 677 (1998).
- [10] H. Jalili, N. F. Heinig, and K. T. Leung, *Phys. Rev. B* **79**, 174427 (2009).
- [11] M. Saloaro, S. Majumdar, H. Huhtinen, and P. Paturi, *EPJ Web. Conf.* **40**, 15012 (2013).
- [12] I. Angervo, M. Saloaro, H. Palonen, S. Majumdar, H. Huhtinen, and P. Paturi, *Phys. Procedia* **75**, 1011 (2015).
- [13] M. Saloaro, M. Hoffmann, W. A. Adeagbo, S. Granroth, H. Deniz, H. Palonen, H. Huhtinen, S. Majumdar, P. Laukkanen, W. Hergert, A. Ernst, and P. Paturi, *ACS Appl. Mater. Interfaces* **8**, 20440 (2016).
- [14] A. S. Ogale, S. B. Ogale, R. Ramesh, and T. Venkatesan, *Appl. Phys. Lett.* **75**, 537 (1999).
- [15] J. Navarro, L. Balcells, F. Sandiumenge, M. Bibes, A. Roig, B. Martínez, and J. Fontcuberta, *J. Phys.: Condens. Matter* **13**, 8481 (2001).
- [16] T. S. Chan, R. S. Liu, G. Y. Guo, S. F. Hu, J. G. Lin, J. M. Chen, and J. P. Attfield, *Chem. Mater.* **15**, 425 (2003).
- [17] S. Colis, D. Stoeffler, C. Mény, T. Fix, C. Leuvrey, G. Pourroy, A. Dinia, and P. Panissod, *J. Appl. Phys.* **98**, 033905 (2005).
- [18] A. Kahoul, A. Azizi, S. Colis, D. Stoeffler, R. Moubah, G. Schmerber, C. Leuvrey, and A. Dinia, *J. Appl. Phys.* **104**, 123903 (2008).
- [19] R. Mishra, O. D. Restrepo, P. M. Woodward, and W. Windl, *Chem. Mater.* **22**, 6092 (2010).
- [20] A. B. Muñoz-García, M. Pavone, and E. A. Carter, *Chem. Mater.* **23**, 4525 (2011).
- [21] D. Stoeffler and S. Colis, *J. Magn. Magn. Mater.* **290-291**, 400 (2005).
- [22] Y. Zhang, V. Ji, and K.-W. Xu, *J. Alloys Comp.* **648**, 374 (2015).
- [23] A. M. Reyes, Y. Arredondo, and O. Navarro, *J. Phys. Chem. C* **120**, 4048 (2016).
- [24] J. Töpfer, R. Kircheisen, and S. Barth, *J. Appl. Phys.* **105**, 07D712 (2009).
- [25] H. Deniz, D. Preziosi, M. Alexe, and D. Hesse, *J. Appl. Phys.* **121**, 023906 (2017).
- [26] D. Serrate, J. M. D. Teresa, and M. R. Ibarra, *J. Phys.: Condens. Matter* **19**, 023201 (2007).
- [27] O. Erten, O. N. Meetei, A. Mukherjee, M. Randeria, N. Trivedi, and P. Woodward, *Phys. Rev. B* **87**, 165105 (2013).
- [28] S. Y. Gómez and D. Hotza, *Renew. Sust. Energ. Rev.* **61**, 155 (2016).
- [29] H. Li, Y. Zhao, Y. Wang, and Y. Li, *Catal. Today* **259**, 417 (2016).
- [30] G. Miao, C. Yuan, T. Chen, Y. Zhou, W. Zhan, and S. Wang, *Int. J. Hydrogen Energy* **41**, 1104 (2016).
- [31] A. B. Muñoz-García, A. M. Ritzmann, M. Pavone, J. A. Keith, and E. A. Carter, *Acc. Chem. Res.* **47**, 3340 (2014).
- [32] L. V. Kovalev, M. V. Yarmolich, M. L. Petrova, J. Ustarroz, H. A. Terryn, N. A. Kalanda, and M. L. Zheludkevich, *ACS Appl. Mater. Interfaces* **6**, 19201 (2014).
- [33] T. Fix, D. Stoeffler, S. Colis, C. Ullhaq, G. Versini, J. P. Vola, F. Huber, A. Dinia, C. Ullhaq, G. Versini, J. P. Vola, F. Huber, and A. Dinia, *J. Appl. Phys.* **98**, 023712 (2005).
- [34] R. Lu, H. Wu, Y. Qian, E. Kan, Y. Liu, W. Tan, C. Xiao, and K. Deng, *Solid State Commun.* **191**, 70 (2014).
- [35] U. Aschauer, R. Pfenninger, S. M. Selbach, T. Grande, and N. A. Spaldin, *Phys. Rev. B* **88**, 054111 (2013).
- [36] U. Aschauer, N. Vonrüti, and N. A. Spaldin, *Phys. Rev. B* **92**, 054103 (2015).
- [37] M. Hoffmann, V. N. Antonov, L. V. Bekenov, K. Kokko, W. Hergert, and A. Ernst, *J. Phys.: Condens. Matter* **30**, 305801 (2018).
- [38] G. Kresse and J. Hafner, *Phys. Rev. B* **47**, 558 (1993).
- [39] G. Kresse and J. Furthmüller, *Comput. Mater. Sci.* **6**, 15 (1996).
- [40] See Supplemental Material at <http://link.aps.org/supplemental/10.1103/PhysRevMaterials.2.083604> for details about the computational setup, the electronic structure of SFMO, and the calculation of defect formation energies.
- [41] K. Momma and F. Izumi, *J. Appl. Crystallogr.* **44**, 1272 (2011).

- [42] K. Schwarz and P. Mohn, *J. Phys. F: Met. Phys.* **14**, L129 (1984).
- [43] P. M. Marcus and V. L. Moruzzi, *J. Appl. Phys.* **63**, 4045 (1988).
- [44] V. L. Moruzzi, P. M. Marcus, K. Schwarz, and P. Mohn, *Phys. Rev. B* **34**, 1784 (1986).
- [45] T. Saitoh, M. Nakatake, A. Kakizaki, H. Nakajima, O. Morimoto, S. Xu, Y. Moritomo, N. Hamada, and Y. Aiura, *Phys. Rev. B* **66**, 035112 (2002).
- [46] I. V. Solovyev, *Phys. Rev. B* **65**, 144446 (2002).
- [47] Z. Szotek, W. M. Temmerman, A. Svane, L. Petit, and H. Winter, *Phys. Rev. B* **68**, 104411 (2003).
- [48] P. E. J. S. Zhang, L. D. Yao, F. Y. Li, Z. X. Bao, J. X. Li, Y. C. Li, J. Liu, C. Q. Jin, and R. C. Yu, *J. Mater. Sci.* **41**, 7374 (2006).
- [49] P. Zhao, R. C. Yu, F. Y. Li, Z. X. Liu, M. Z. Jin, and C. Q. Jin, *J. Appl. Phys.* **92**, 1942 (2002).
- [50] D. D. Taylor, N. J. Schreiber, C. M. Brown, A. M. Arevalo-Lopez, and E. E. Rodriguez, *Chem. Comm.* **51**, 12201 (2015).
- [51] O. Chmaissem, R. Kruk, B. Dabrowski, D. E. Brown, X. Xiong, S. Kolesnik, J. D. Jorgensen, and C. W. Kimball, *Phys. Rev. B* **62**, 14197 (2000).
- [52] L. Shi, L. Wu, Y. F. Duan, J. Hu, X. Q. Yang, G. Tang, and L. Z. Hao, *Eur. Phys. J. B* **86**, 9 (2013).
- [53] M. Faizan, G. Murtaza, S. H. Khan, A. Khan, A. Mehmood, R. Khenata, and S. Hussain, *Bull. Mater. Sci.* **39**, 1419 (2016).
- [54] S. K. Nayak, H. T. Langhammer, W. A. Adeagbo, W. Hergert, T. Müller, and R. Böttcher, *Phys. Rev. B* **91**, 155105 (2015).
- [55] K. Reuter and M. Scheffler, *Phys. Rev. B* **65**, 035406 (2001).
- [56] M. Hagen and M. W. Finnis, *Philos. Mag. A* **77**, 447 (1998).
- [57] J. A. Santana, R. Mishra, J. T. Krogel, A. Y. Borisevich, P. R. C. Kent, S. T. Pantelides, and F. A. Reboredo, *J. Chem. Theory Comput.* **13**, 5604 (2017).
- [58] Y. Huan, Y. Li, B. Yin, D. Ding, and T. Wei, *J. Power Sources* **359**, 384 (2017).
- [59] J. Navarro, C. Frontera, L. Balcells, B. Martínez, and J. Fontcuberta, *Phys. Rev. B* **64**, 092411 (2001).
- [60] J. Santiso, A. Figueras, and J. Fraxedas, *Surf. Interface Anal.* **33**, 676 (2002).
- [61] J. Raittila, T. Salminen, T. Suominen, K. Schlesier, and P. Paturi, *J. Phys. Chem. Solids* **67**, 1712 (2006).
- [62] L. Harnagea and P. Berthet, *J. Solid State Chem.* **222**, 115 (2015).